Single-Chip Multiple-Frequency ALN MEMS Filters Based on Contour-Mode Piezoelectric Resonators

Gianluca Piazza, *Member, IEEE*, Philip J. Stephanou, *Member, IEEE*, and Albert P. (Al) Pisano

Abstract—This paper reports experimental results on a new class of single-chip multiple-frequency (up to 236 MHz) filters that are based on low motional resistance contour-mode aluminum nitride piezoelectric micromechanical resonators. Rectangular plates and rings are made out of an aluminum nitride layer sandwiched between a bottom platinum electrode and a top aluminum electrode. For the first time, these devices have been electrically cascaded to yield high performance, low insertion loss (as low as 4 dB at 93 MHz), and large rejection (27 dB at 236 MHz) micromechanical bandpass filters. This novel technology could revolutionize wireless communication systems by allowing cofabrication of multiple frequency filters on the same chip, potentially reducing form factors and manufacturing costs. In addition, these filters require terminations (1 kΩ termination is used at 236 MHz) that can be realized with on-chip inductors and capacitors, enabling their direct interface with standard 50-Ω systems.   [2006-0051]

Index Terms—Aluminum nitride (AlN), contour-mode resonators, ladder filters, microelectromechanical systems (MEMS) filters, microelectromechanical systems (MEMS) resonators, piezoelectric resonators.

I. INTRODUCTION

A S THE DEMAND for ubiquitous connectivity grows, the expectations of wireless appliance's functionalities are becoming increasingly exacting. Radio frequency (RF) microelectromechanical systems (MEMS) is an emerging technology that promises to enable both new RF system architectures and unprecedented levels of performance and integration. The principal drivers of research in RF-MEMS resonator technology are resonator-based circuits, namely filters and oscillators. Solutions capable of integrating multiband and multistandard devices that consume low power and have small form factors will accomplish the vision of next-generation, ubiquitous wireless communications.

Several research groups [1]–[7] have demonstrated coupled electrostatically driven microresonators for filtering applications. Although characterized by very high Q, these microdevices suffer from large motional resistance, R_M. For

filters, a large R_M translates either into the need for bulky matching elements or large insertion losses and makes these resonators unintegrable with existing 50-Ω systems. Recent research results [8]–[12] have shown the ability to lower the motional resistance of these microresonators by using "internal" electrostatic transduction. Although promising, this technology remains unproven and must contend with large capacitances. Piezoelectric materials such as aluminum nitride or quartz offer larger electromechanical coupling coefficients that reduce the motional resistance of the resonators to a few ohms and provide large bandwidths for filtering applications. Piezoelectric resonators, such as film bulk acoustic resonators (FBARs) [13]–[19] have been successfully demonstrated and electrically cascaded to form bandpass filters in the GHz range. Because the film thicknesses determine the center frequency of these resonators, multiple-frequency filtering solutions based on FBARs cannot be economically manufactured as single-chip RF modules.

For the first time, this paper realizes monolithic integration of multiple-frequency aluminum nitride (AlN) bandpass filters, which represents a major breakthrough towards the goal of highly integrated, single-chip, multiband solutions. Using a new class of MEMS resonator technology based on the excitation of contour modes of vibration in AlN microstructures [17], bandpass filters at 93 and 236 MHz have been demonstrated by electrically cascading up to eight resonators in a ladder topology. These filters show very promising performance, being characterized by low insertion losses (4 dB at 93 MHz), large close-in and out-of-band rejection (~40 and ~27 dB, respectively, for a 93–MHz filter) and fairly sharp roll-off with a 20 dB shape factor of 2.2. The filters described in this paper are about 20× smaller than existing surface acoustic wave (SAW) device based implementations. In addition, the −25 ppm/ °C temperature coefficient of contour mode AlN filters results in 40% lower temperature sensitivity than some of their (e.g., $LiTaO_3$) SAW counterparts.

II. RESONATOR ARRAYS

Vast amounts of research in the field of electromechanical resonators for filtering applications has generated different techniques for realizing bandpass filters. The same fundamental methods that have undergone refinement and innovation for over 60 years [20]–[22] are still the preferred implementations for bandpass filters using resonators. There are two main approaches:

1) electrically coupled filters, in which an array of resonators is coupled together exclusively by electrical signals; the resonators are cascaded in series and parallel branches to
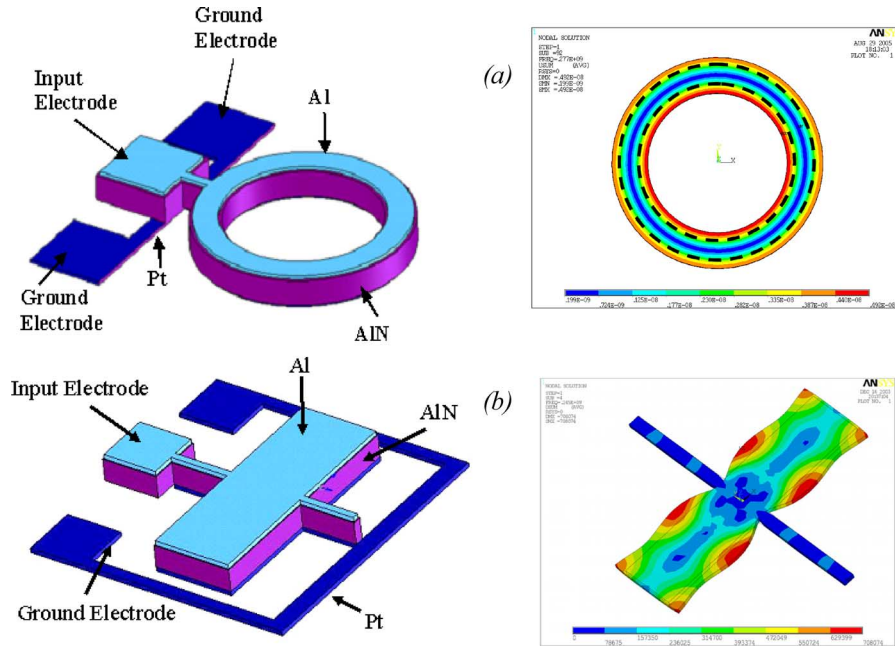
Fig. 1. Schematic views of the building blocks for the filters and their mode shapes. (a) Circular ring AlN resonator excited in a radial-extensional contour mode shape as shown in ANSYS plot. (b) Rectangular plate AlN resonator excited in a width-extensional contour mode shape as shown in ANSYS plot.

form either by themselves or with external passive components (inductors and capacitors) L, PI, or T networks;

2) mechanically coupled filters, in which arrays of resonators are coupled by purely mechanical links; different arrangements of resonators are possible so that fully mechanical signal processing functions can be implemented. The electrical signal is simply used to excite the input of the structure and is picked off at the output stage, whereas the bandpass function is constructed by purely mechanical interactions between the resonators.

Between the two approaches, electrical coupling of resonators allows the advantage of simpler implementation. There is no need for external mechanical links, which are generally very challenging to manufacture especially at high frequencies. The size of the link is generally a fraction of the resonator size ($\sim$1/10) and at 1 GHz could translate into critical dimensions below 0.5 μm. In addition, electrical cascading of resonators offer rapid implementation of complex designs with zeros (also known as attenuation poles) in the filter transfer function. Advantages of mechanically coupled resonators include the ability to set the bandwidth of the filter independently of material properties [23] and the ability to improve out-of-band rejection. Theoretically the use of mechanically coupled resonators eliminates the limit on the maximum achievable bandwidth imposed by the material properties, and increases the out-of-band rejection by eliminating the parallel capacitance of the device. Thus a hybrid solution that combines mechanical and electrical coupling of resonators might be very intriguing, especially for contour mode resonators. In this paper, because of their ease of design and fabrication, electrically coupled resonators are presented as an example of the implementation of IF filters. The following sections provide details on the design and experimental characterization of these filters.

III. DESIGN OF ELECTRICALLY COUPLED FILTERS

The AlN resonators are formed by a thin (2 μm) AlN film sandwiched between a bottom platinum (Pt) electrode and a top aluminum (Al) electrode. By applying an electric field across the film thickness, the resonator is excited in lateral vibrations by means of the d_{31} piezoelectric coefficient. The contour-mode rectangular plate and ring-shaped AlN resonators shown in Fig. 1 are the building blocks for the bandpass filters of this paper. The basic ladder filter configuration is composed of cascaded L networks (Fig. 3), each formed by series and shunt resonators. Such networks can be cascaded to form PI and T networks and other more complicated multipole filters.

In order to analyze these networks, a concise way of describing the equivalent electrical impedance Z_R of each one-port resonator is adopted [based on the Butterworth Van Dyke (BVD) model] [24]

$$Z_R = \frac{1}{j\omega C_o} \frac{z_S}{z_P}$$
$$z_S = 1 - \left(\frac{f}{f_S}\right)^2 + j\left(\frac{f}{f_S}\right)\Big/Q_S$$
$$z_P = 1 - \left(\frac{f}{f_P}\right)^2 + j\left(\frac{f}{f_P}\right)\Big/Q_P \qquad (1)$$

where f_S and f_P are the series and parallel resonant frequencies, Q_S and Q_P are the resonator's quality factor for the series and parallel resonances, and C_o, is the parallel capacitance of the BVD model shown in Fig. 2. C_o is used instead of an equivalent low frequency capacitance as reported in [24] because the two only differ by approximately 1%.
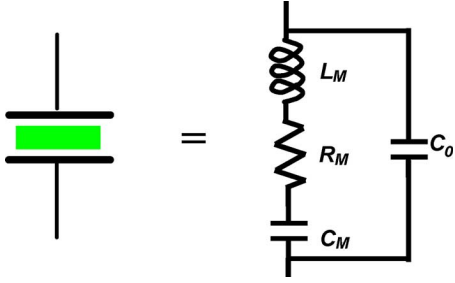
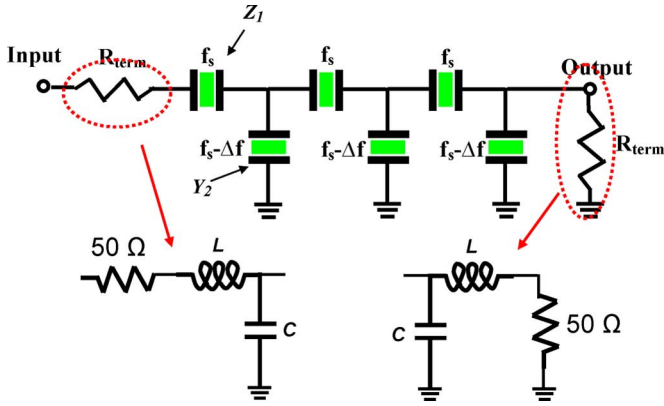Fig. 2. Schematic representation of a piezoelectric resonator and equivalent BVD circuit representation.

Fig. 3. Schematic representation of a ladder filter structure made out of three cascaded L networks. *LC* matching elements can be used to implement the termination resistance and directly couple the system match to 50 Ω.

Adopting the ABCD matrix approach [25], each L section can be described in the following way:

$$\begin{bmatrix} A & B \\ C & D \end{bmatrix} = \begin{bmatrix} 1 + Y_2 Z_1 & Z_1 \\ Y_2 & 1 \end{bmatrix} \qquad (2)$$

where

$$Z_1 = \frac{1}{j\omega C_1}\frac{z_{S1}}{z_{P1}} \quad Y_2 = j\omega C_2 \frac{z_{P2}}{z_{S2}} \qquad (3)$$

and the subscript 1 refers to the series branch resonator and 2 to the shunt branch resonator. C_1 and C_2 represent the resonator parallel capacitance C_o, respectively, for the series branch and the shunt branch resonators. Therefore, using the correspondence between ABCD matrix elements and scattering parameters [25] it is possible to derive the scattering parameter of an L section. Specifically, S_{21} is given by (4), shown at the bottom of

the page, where R_{term} is the termination resistance. By simply cascading one section after the other one can construct more complex filter structures

Equation (4) shows a maximum when the series resonance of the series branch, f_{S1}, coincides with the parallel resonance of the shunt branch, f_{P2}. In order to correctly match the filter characteristic impedance at its center frequency, the termination resistance R_{term} should be chosen to be [26]

$$R_{\mathrm{term}} \approx \frac{1}{\omega\sqrt{C_1 C_2}} \approx R_M \frac{Q_{\mathrm{RES}}}{Q_{\mathrm{FLTR}}} = \frac{M_{\mathrm{RES}}}{\eta_{\mathrm{RES}}^2} BW_{\mathrm{FLTR}} \quad (5)$$

where Q_{RES} and Q_{FLTR} are the quality factor of the single resonator and of the filter (3 dB bandwidth of filter), respectively, M_{RES} is the equivalent mass of the resonator, η_{RES} is the electromechanical coupling factor for the resonator [27], specifically $\eta_{\mathrm{RES}} = 2E_P d_{31} L$ for a rectangular plate resonator, E_P being the AlN Young's moduls, d_{31} is the piezoelectric coefficient, and L is the length of the plate, and BW_{FLTR} is the 3 dB filter bandwidth. It is clear from (5) that a large R_M requires multiple matching stages that introduce loss. At the same time, high Q cannot compensate for small electromechanical coupling (typical of electrostatically driven resonators) to reduce R_{term} for a given filter bandwidth.

For a given value of R_{term}, the insertion losses IL of the filter can be expressed in the following way:

$$IL \approx 1 - \frac{n}{4\pi f_C C_1 R_{\mathrm{term}} k_t^2 Q_{\mathrm{RES}}} \qquad (6)$$

where k_t^2 is the effective electromechanical coupling coefficient and n refers to the number of series resonators that are cascaded to form the filter. k_t^2, which describes the internal conversion between electrical and mechanical energy, is a material dependent property that does not depend on the specific geometry of the transducer under consideration (k_t^2 is different from η_{RES})

$$k_t^2 = \frac{d_{ij}^2}{\varepsilon_i s_{jj}} \qquad (7)$$

where d_{ij} is the specific piezoelectric coefficient in use (d_{31} for contour-mode resonators), ε_i is the dielectric permittivity of the piezoelectric material, and s_{jj} is its compliance. Because of its generality, k_t^2 is considered an important figure of merit in estimating the performance of a resonator for filtering applications. k_t^2 does not only affect the IL of the filter, but also sets its fractional bandwidth (9). Out-of-band rejection of a ladder filter can be computed from (4) when the frequency is far from the filter's

$$S_{21} = \frac{2}{A + D + B/R_{\mathrm{term}} + C R_{\mathrm{term}}}$$

$$S_{21} = \frac{2j\omega C_1 z_{P1} z_{S2}}{2j\omega C_1 z_{P1} z_{S2} + j\omega C_2 z_{S1} z_{P2} + z_{S1} z_{S2}/R_{\mathrm{term}} - \omega^2 C_2 C_1 z_{P2} z_{P1} R_{\mathrm{term}}} \qquad (4)$$
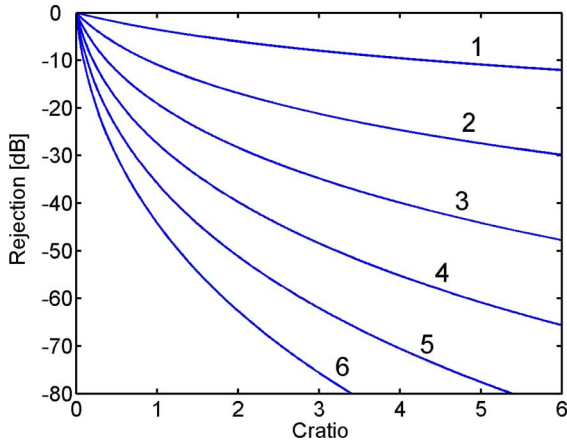
Fig. 4. Effect of capacitance ratio (between parallel and series branches) and number of L sections (here varying between 1 and 6) on the out-of-band rejection.
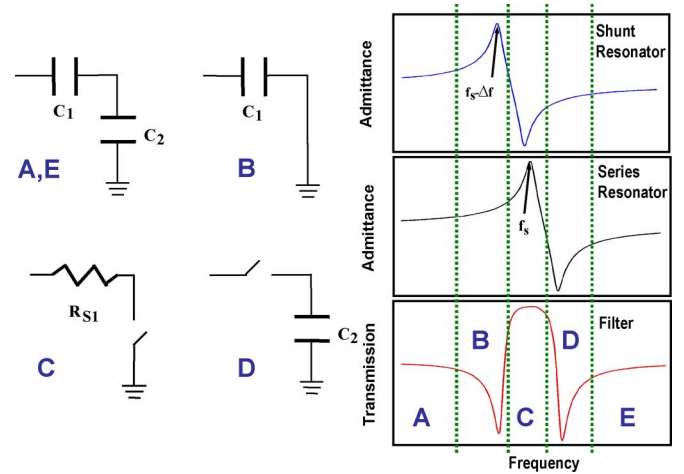

Fig. 5. Intuitive explanation of the principle of operation of the L section used as a building block in ladder filters. Five principle areas of operation have been identified and the corresponding equivalent circuit of each of the resonators has been highlighted.

center frequency. The out-of-band value of S_{21} for n L stages is approximately

$$S_{21}\text{\_Out-of-Band} \approx \frac{1}{\left(1 + \frac{C_2}{C_1}\right)^n} \qquad (8)$$

and depends primarily on the capacitance ratio of the resonators in the shunt and series branches. The dependence of the out of band rejection on the capacitor ratio and the number of L sections is shown in Fig. 4 [exact calculation based on (4) was used in Fig. 4].

A particular feature of the ladder filter transfer function is the presence of two zeros, coinciding, respectively, with the series resonance of the shunt resonator f_{S2} and the parallel resonance of the series resonator, f_{P1}. These zeros provide for sharp roll-off of the filter and high close-in-band rejection. This feature is particularly important when designing duplexers, which demand large isolation between closely spaced transmitting and receiving channels. These zeros also set the fractional bandwidth of the filter according to

$$\frac{f_{P1} - f_{S2}}{f_C} \approx \frac{8}{\pi^2} k_t^2. \qquad (9)$$

Based on (9), the maximum achievable fractional bandwidth for contour-mode resonators is about 2.5%. Therefore, unless a hybrid approach that uses both mechanically and electrically coupled resonators is adopted, it is problematic to obtain the larger fractional bandwidths (up to 3%) that cellular standards such as PCS, GSM, and WCDMA require for RF filters. The behavior of the L section of a ladder filter can be described in an intuitive manner as depicted in Fig. 5. Far from resonance (region A and E), the two resonators behave as capacitor, and the transfer function is given by the ratio of the two capacitors. At the series resonance (region B) of the shunt resonator, f_{S2}, the shunt resonator behaves as a very small resistance to ground, yielding a zero in the transfer function. Similarly at the parallel resonance (region D) of the series resonator, f_{P1}, the series resonator can be approximated by an open (very large resistance) and again

a zero appears in the filter transfer function. In the pass band (region C) the series resonators show a minimum resistance responsible for the insertion losses, whereas the shunt branches behave as open circuits.

According to the aforementioned derivations, the designer has a set of parameters with which to prescribe the performance of a ladder filter:

1) the center frequency by properly selecting the desired contour geometry;
2) the capacitance ratio between the series and parallel branches. This choice affects not only the out-of-band rejection, but also the insertion losses, termination resistance, geometry and motional resistance. In addition, in some solutions [28], instead of including different size resonators, it is advisable to employ two resonators of the same size coupled in series or parallel in order to reduce or increase the effective capacitance;
3) the number of stages and the number of resonators in the series and parallel branches. The number of stages directly affects the order of the filter and therefore its roll-off and shape factor. The number of series and parallel resonators to be employed affects the overall size of the filter and changes the actual shape of the transfer function (Fig. 6). Several solutions are possible from this point of view and are generally dictated by a tradeoff between space savings and satisfying the specifications of the relevant standards.

IV. FREQUENCY SHIFT

An important feature for the implementation of ladder filters is the ability to manufacture resonators with different resonant frequencies for the series and shunt branches; such difference needs to be comparable to the 3 db bandwidth of the filter. As outlined in the previous section, it is of fundamental importance to have the series resonance of the series resonator overlapping with the parallel resonance of the shunt resonator. Depending on the bandwidth specification, this may require a frequency shift in the range of 0.1% and 3%.
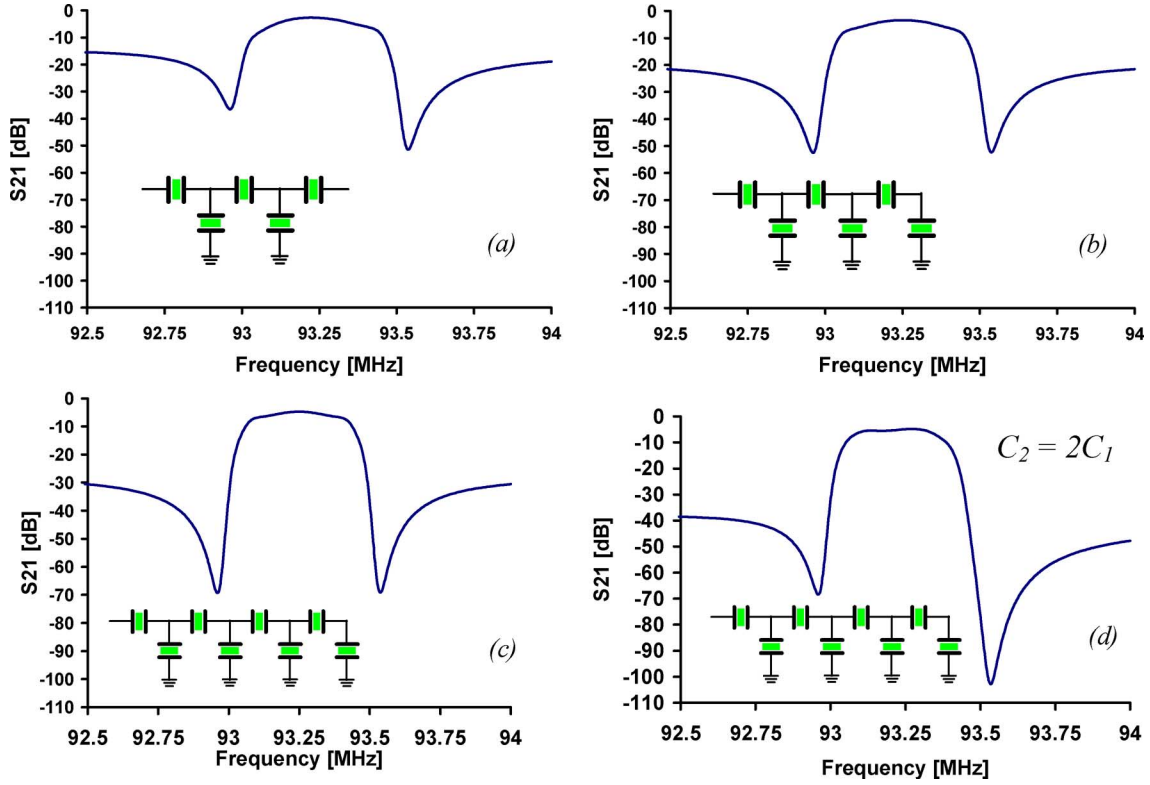
Fig. 6.   Simulated S_{21} response of a 93–MHz filter implemented using rectangular plate resonators having individual Q of 2000 and R_M of 300 Ω. The termination resistors were selected according to equation (5). (a) Electrical response of 3/2 ladder structure showing asymmetry and poor out-of-band rejection. (b) Electrical response of 3/3 ladder structure showing higher rejection and symmetrical response. (c) Electrical response of 4/4 ladder structure; higher out-of-band rejection is obtained, but insertion losses are increased with respect to (b). (d) Electrical response of 4/4 ladder structure for which a cap ratio of 2 between the parallel and series branches was selected [C_1 and C_2 as defined in (3)]. This configuration improves out-of-band rejection with a small increase in insertion loss.

Although the frequency of contour-mode resonators is determined by the in-plane geometrical dimensions of the structure, it is not practical to define such a small shift by simply changing the dimensions of the structure at the CAD level. This change would in fact require prohibitively expensive submicron accuracy on the lithography equipment. The preferred solution involves exploiting the mass loading caused by the Pt electrode. Pt has a mass density which is about 6.5 times that of AlN. By lithographically removing small amounts of Pt it is possible to raise the center frequency of the resonator. This is a significant feature of the present paper, because it allows the desired frequency shift to be implemented at the mask layout level, thereby obviating the need for additional deposition steps as is generally required for thickness mode resonators. This solution drastically simplifies the fabrication process making it more robust and economical. It is worth noting from Fig. 7 (cross-sectional view of a ring) that the removal of Pt occurs at the location of minimum strain. According to the piezoelectric equations [29], we can remove small amounts of Pt without affecting the electrical transfer function of the resonator because minimal motional charge is generated at these locations.

The analysis of the frequency shift induced by Pt is presented below. Selectively removing Pt in a pattern that is perpendicular to the direction of bulk acoustic wave propagation in the piezoelectric medium allows us to use a very simple modeling approach based on [30]. This approach proves valid when removing a small amount of Pt from the length of a rectangular
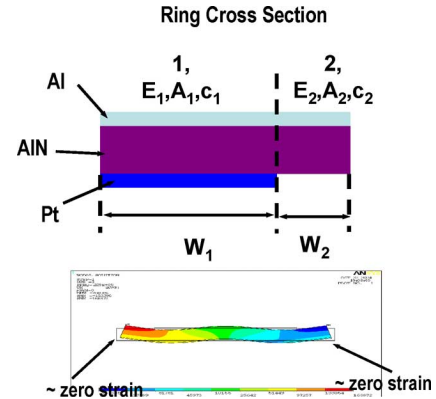

Fig. 7.   Cross-sectional view of circular ring structure illustrating the location where Pt is lithographically removed in order to induce the desired frequency shift. Note that the Pt is removed at the location of minimum or almost zero strain as shown by cross-sectional view of resonator mode shape in ANSYS.

plate excited in a width-extensional mode. In this case we can find that the frequency of vibration is given by [30]

$$f_{\text{NEW}} = f_o \sqrt{\frac{\left(1 + \frac{E_{Pt} A_{Pt}}{E_R A_R}\right)}{\left(1 + \frac{\rho_{Pt} A_{Pt}}{\rho_R A_R}\right)}} \qquad (10)$$

where f_o is the resonator center frequency without any metal; E, A, and ρ are the equivalent Young's modulus, cross-sectional

area and mass density of either platinum (subscript Pt) or the piezoelectric material (subscript R). By changing the length of the Pt electrode, the effective area of the Pt layer A_{Pt} changes and according to (10) the resonator frequency can be raised. It is possible to induce a frequency shift of 500 ppm for every μm of Pt that is removed from the length of a $200 \times 50 \ \mu$m rectangular plate having a 100–nm-thick Pt electrode.

The case of the ring, as shown in Fig. 7, is different because the removal of Pt occurs in the same direction of propagation of the bulk wave. The problem needs to be handled as a two-part composite rod undergoing longitudinal vibrations [31]. In this case we need to define an equivalent "EA" (product of Young's modulus time the cross-sectional area) and an equivalent acoustic velocity for sections 1 and 2 in Fig. 7. Therefore, (Al electrode is considered negligible in this analysis)

$$E_1 A_1 = E_{Pt} A_{Pt} + E_P A_P \quad E_2 A_2 = E_P A_P$$
$$A_{Pt} = T_{Pt} 2\pi R_{AVE} \quad A_P = T_P 2\pi R_{AVE}$$
$$c_1 = \sqrt{\frac{E_1 A_1}{\rho_{Pt} A_{Pt} + \rho_P A_P}} \quad c_2 = \sqrt{\frac{E_2 A_2}{\rho_P A_P}} = \sqrt{\frac{E_P}{A_P}} \quad (11)$$

where each area A is an approximate value based on a circular ring geometry, valid for rings with $R_{AVE} \gg W$ and T_{Pt} is the thickness of the Pt electrode.

The frequency equation is given by [31]

$$\frac{E_2 A_2}{E_1 A_1} \cos\left(\frac{\omega}{c_1} W_1\right) \sin\left(\frac{\omega}{c_2} W_2\right) +$$
$$\cos\left(\frac{\omega}{c_2} W_2\right) \sin\left(\frac{\omega}{c_1} W_1\right) = 0 \quad (12)$$

where ω is the unknown resonant frequency and W_1 and W_2 are the width of each section, respectively. According to (12), when small amounts of Pt are removed, variations in the resonator center frequency with respect to W_2 can be approximated to have a linear dependence on W_2. Calculations show that for a 100–nm-thick Pt electrode the center frequency of a 90-μm inner radius ring structure shifts by ~7000 ppm for each μm of Pt that is removed from the width of the structure.

A second method to obtain the desired frequency shift is to use in the series and parallel branches rings with different average diameters or rectangular plates with different aspect ratios. It can be shown (Fig. 8) [32] that the resonant frequency of circular rings is a weak function of the average radius. A decrease in resonant frequency of 0.7% is recorded when R_{AVE} is increased by three times (from 50 to 150 μm). At the same time, this approach permits one to design different capacitance ratios between the series and shunt resonators, improving the out-of-band rejection, as previously shown in Fig. 6. In contrast to the approach based on Pt etching, this method requires relatively large layout area to define significant (1%–2%) frequency shifts and reduces the designer's freedom of setting bandwidth independently of capacitance ratio.

V. FILTER FABRICATION

The process employed for fabricating the resonant microstructures of this paper is based on surface micromachining techniques that are compatible with state-of-the-art CMOS production systems. The metallization steps are conventional
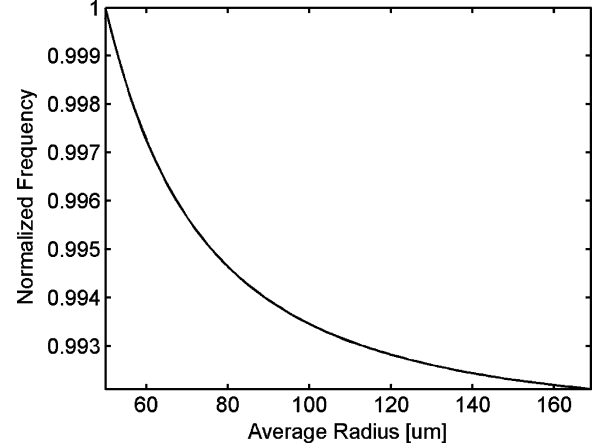

Fig. 8. Frequency variation versus average radius of a 20–μm-wide circular ring. Frequency is normalized to the value for a ring with 50-μm average radius. Rings with larger average radius have lower resonant frequency.

micromachining processes. Although compatible with CMOS fabrication, the etching of AlN and the release of the microstructures can be considered somewhat exotic. In the last decade etching of some III-V compounds such as AlN and XeF_2 release are gaining wider use and understanding, but they are still considered unproven for high yield and large volume manufacturing. Despite these issues, the fabrication process of these filters is very robust and very easily implemented.

A simple four-mask process has been used to fabricate the filters (Fig. 9). Two μm AlN film is sandwiched between a bottom platinum electrode and a top aluminum electrode. The fabrication process starts by patterning the bottom Pt electrode (approximately 100 nm) on a low stress nitride (LSN) buffer layer in order to reduce parasitic capacitance and electrical losses. The Pt electrode is deposited by RF sputtering and patterned by lift off. The patterning of the Pt electrode improves not only the electrical isolation to the substrate, but also the quality (degree of orientation) of the AlN films. AlN films are sputter-deposited using a single-module Advanced Modular Sputtering (AMS, Goleta, CA) PVD sputtering tool. A wet etch step in 160 °C phosphoric acid is used to access the bottom electrode. The wet etch step provides for low-slope profiles so that contact between thin Al layers (150–175 nm thick) and Pt bottom electrode is easily achieved. Fig. 9 shows a side and front view of the contact. Unfortunately the deposition of 400 °C low-temperature oxide (LTO) masking layer for the AlN etch seems to affect the surface roughness of the contact. It is believed that a platinum aluminide alloy forms when the two contacting materials are exposed to high temperatures (see phase diagram of Pt and Al in [33]). Despite the roughness, the electrical quality of the contact is preserved. The top Al electrode is patterned by dry etching. Cl_2-based dry etching is used to pattern AlN. The top Al electrode is protected by a thin (approximately 30 nm) layer of Nb that is removed with the remaining oxide during a CF_4-based dry etch step. This step selectively removes the masking layer and etches the remaining LSN without attacking the resonant structure. The selectivity between LTO and AlN during the Cl_2-based dry etch process is about 1:3. The structures are released by dry etching of silicon in XeF_2, which
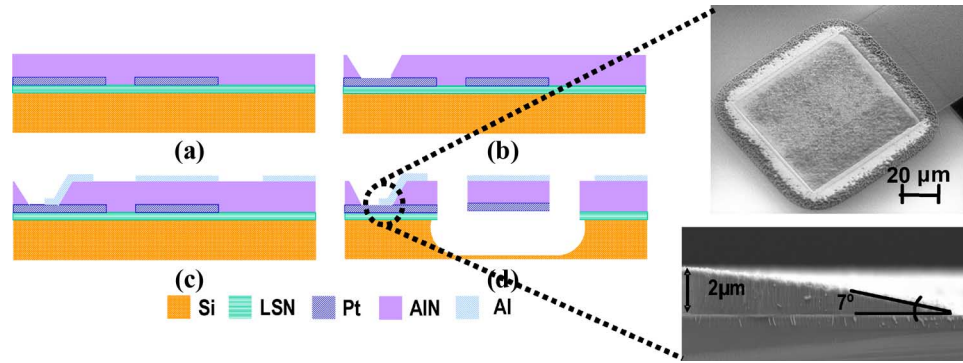
Fig. 9. Fabrication process used for the realization of ladder filters. (a) Low stress nitride (LSN) deposition by LPCVD, followed by Pt patterning by lift-off and AlN sputter deposition. (b) Open via access to bottom Pt electrode through AlN. AlN is wet etched by 160 °C H_3PO_4. (c) Deposition of top Al electrode and patterning by dry etching in Cl_2-based chemistry. (d) Cl_2-based dry etching of AlN resonant devices and dry release in XeF_2. The inset SEMs show top and side views of the Al to Pt contact.
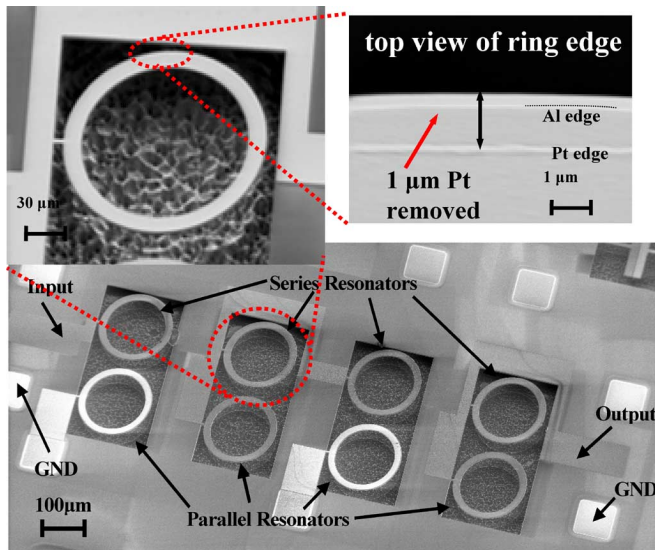

Fig. 10. SEM image of a fourth-order ladder filter made out of eight identical circular rings. The process-defined frequency shift defined by the removal of 1 μm of Pt from the series resonator is highlighted in the close-up views.

is extremely selective to AlN, Al, and Pt, and solely removes Si and LSN (generally low-Q material) present underneath the structure.

VI. EXPERIMENTAL RESULTS

The fabricated micromechanical filters were tested in an RF probe station at atmospheric pressure. Ground-signal-ground (GSG) probes were used. Two-port S-parameter calibration based on short, open, load, and through (SOLT) standards on a Picoprobe (GGB Industries, Inc., Naples, FL) ceramic substrate was performed. Full S-parameter matrices were extracted for each filter using an Agilent E5071B network analyzer (Agilent Technologies, Santa Clara, CA). No external terminations were connected to the device under test. The network analyzer allows automatic change of the filter terminations and computation of the transmission spectrum.

Eight rings (Fig. 10), all with an inner radius of 90 μm and 20 μm wide, were electrically cascaded in a ladder structure. The frequency of the series and shunt branches were shifted by

approximately 0.3%. It is important to note that a wider bandwidth could be obtained, but extra parasitic capacitance introduced by the fabrication process and the test fixture limited the overall bandwidth. This filter shows moderate insertion losses of -7.9 dB at 236.2 MHz, an out-of-band rejection of 26 dB and a 20 dB shape factor of 2.79 (Fig. 11). It is interesting to note that this filter does not suffer from any other spurious resonance (Fig. 11). The non-ideal shape factor is due to slight mismatches in frequency between adjacent resonators. The agreement between experimental and theoretical results (obtained by cascading ABCD parameters in (2) is not perfect because parasitic capacitances were not modeled and it was not possible to measure the quality factor and motional resistance of each resonator and eventual mismatch between resonators. It is important to note that a termination of only 1 kΩ was required for this filter. This value translates into L and C components (Fig. 3) of 147 nH and 2.9 pF, respectively, values that can be realized by on-chip inductors and capacitors. The combination of on-chip matching to 50 Ω and relatively low insertion losses are the key features of these IF filters. The most important filter performance are also summarized in Table I, where experimental results are compared to theoretical calculations obtained using (4)–(6) and (8). There is good agreement between theory and experiments.

As discussed previously, the frequency shift was also defined by changing the size of the inner radius of the rings in the shunt branch (average radius of 150 μm was used in the shunt branch and 100 μm in the series branch). Up to six rings were connected in this configuration. Although the results are promising (Fig. 12), large insertion losses ($\sim$11.3 dB) at 236 MHz were recorded, which were attributable to the longer traces needed to connect the resonators. Also, the additional capacitance due to the longer traces affects the out-of-band rejection, negating the effect of an improved capacitance ratio.

Four, six and eight (Fig. 13) 200-μm-long and 50-μm-wide rectangular plates were tested in a ladder configuration as well. Again the frequencies were shifted by about 0.3%. Although this frequency shift is not sufficient to satisfy the standards at RF frequencies, it works well for IF frequencies. An example of the electrical response of eight rectangular resonators is shown in Fig. 14. In this case insertion losses as low as 4 dB were
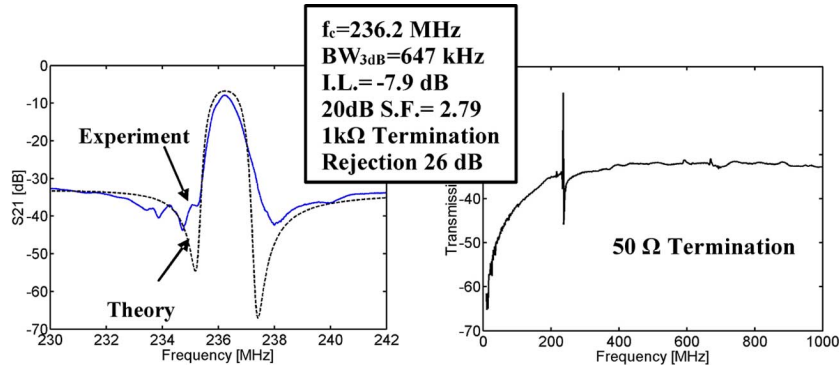
Fig. 11. Electrical response of a bandpass filter constituted by eight ring-shaped resonators arranged in a ladder configuration with termination of 1 kΩ. The resonators had individual Q in on the order of 800. A large scan of the same filter showing no interfering spurious responses was taken from 0 to 1 GHz. 50–Ω terminations were used in this scan (1-GHz-wide scan).

TABLE I
COMPARISON BETWEEN THEORY AND EXPERIMENT OF THE PRIMARY PERFORMANCE PARAMETERS FOR THE 8 RING AND 8 RECTANGULAR PLATE FILTERS THAT WERE PRESENTED IN THIS PAPER AND SHOWN IN FIGS. 10 AND 13, RESPECTIVELY. THEORETICAL CALCULATIONS ARE BASED ON THE EXPERIMENTALLY DERIVED RESONATOR PARAMETERS. FOR THE CIRCULAR RING: $C_o = 0.56\,\text{pF}$, $k_t^2 = 0.43\%$, $Q = 800$. FOR THE RECTANGULAR PLATE: $C_o = 0.81\,\text{pF}$, $k_t^2 = 0.4\%$, $Q = 2000$

Filter Performance	8 Circular Ring Filter		8 Rectangular Plate Filter	
	Theory	Experiment	Theory	Experiment
IL [dB]	- 7.3	- 7.9	- 2.5	- 4
Rejection [dB]	- 20	- 26	- 25	- 27
Termination [Ω]	1200	1000	2110	2000

3+3 rings
Different size ser/shunt
f_c=236 MHz
BW$_{3dB}$=553 kHz
I.L.= -11.3 dB
20dB S.F.= 4.4
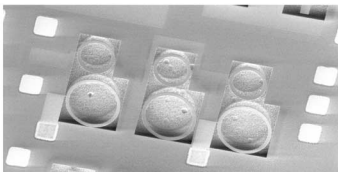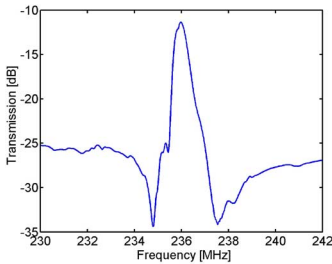1kΩ Termination
Rejection 15 dB

Fig. 12. Electrical response and SEM of a 236-MHz ladder filter realized using different size rings in the series and shunt branches.

recorded at 93.2 MHz and an out-of-band rejection of 27 dB were achieved. As shown in Fig. 14 a second bandpass filter exists due to the length-extensional mode shape present in the plate. This mode could be suppressed by placing the anchors of the plate along the length instead of the width of the structure [34]. For this filter, a 2-kΩ termination was needed. The value is slightly larger than what was recorded for the filters made out of rings and it is because the rectangular plates show slightly larger motional resistance than the rings. Again on-chip inductors and capacitors could be used for matching, with L equal to 530 nH and C to 5.3 pF. Table I compares theory and experiments for the filter composed of eight rectangular plates. Discrepancies in
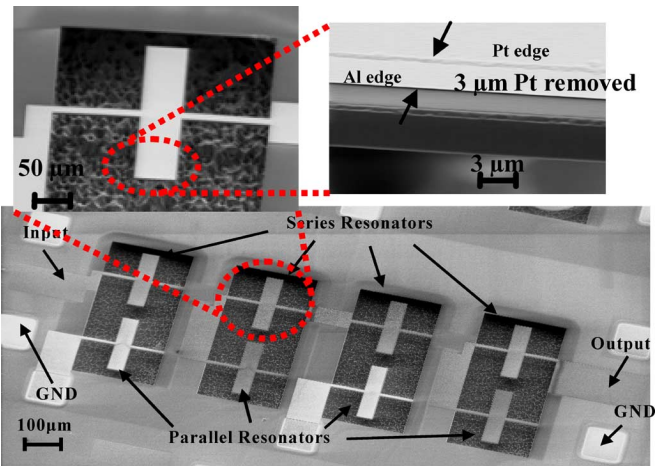

Fig. 13. SEM view of a ladder filter made out of eight electrically cascaded rectangular plate resonators. Zoomed-in view shows details of the single rectangular resonator and lithographically defined variation in bottom electrode length used to tune the center frequency of the series resonators.

the out-of-band rejection are potentially introduced by parasitic capacitances in the shunt branches as for the filter formed by eight rings. The larger than predicted IL are due to performance differences between the different resonators in the filter.

The results for four and six rectangular resonant filters are summarized in Table II. From Table II and Fig. 15 it is evident that a higher-order filter (more L sections) improves the out-of-band rejection at the expenses of larger insertion losses.

These IF filters also showed temperature dependence that is about 40% better than some existing SAW filters. The TCF of each individual resonator is about $-25\,\text{ppm}/\,^\circ\text{C}$. Fig. 16 shows the shift in bandwidth with temperature for a third-order filter that uses six rectangular plates connected in a ladder structure.

VII. CONCLUSION

For the first time, contour-mode AlN piezoelectric resonators have been electrically coupled in a ladder structure to form low insertion loss, bandpass filters at 93 and 236 MHz. Although the performance of these filters are not yet optimized, they represent a major breakthrough toward the realization of single-chip, multifrequency, and integrated bandpass filter solutions characterized by higher performance and smaller form factors than
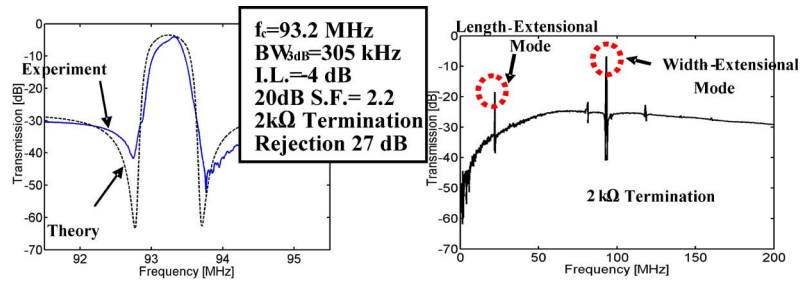
Fig. 14. Electrical response of a 93.2–MHz bandpass filter constituted by eight rectangular resonators arranged in a ladder configuration. Resonators had individual Q in the order of 2000. Large scan of the same filter response from 0 to 200 MHz with 2–kΩ terminations was taken. A length-extensional mode is present together with the width-extensional mode.

TABLE II
RESPONSE PARAMETERS AND CHARACTERISTICS OF BANDPASS FILTERS
BUILT USING RECTANGULAR PLATE RESONATORS

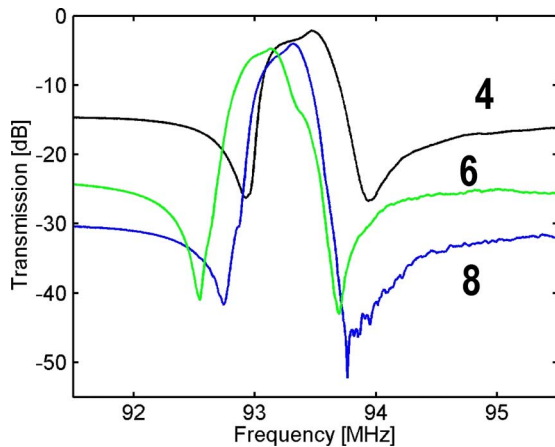| Number of Resonators	f_c [MHz]	BW_{3dB} [kHz]	I.L. [dB]	20dB S.F.	R_{term} [kΩ]
4	93.5	456	-2	N.A.	1.5
6	93.1	332	-4.7	2.7	2

Fig. 15. Electrical response of second-, third-, and fourth-order ladder filters made out of, respectively 4, 6, and 8 rectangular plate resonators. Out-of-band rejection improves with filter order at the expenses of insertion losses.
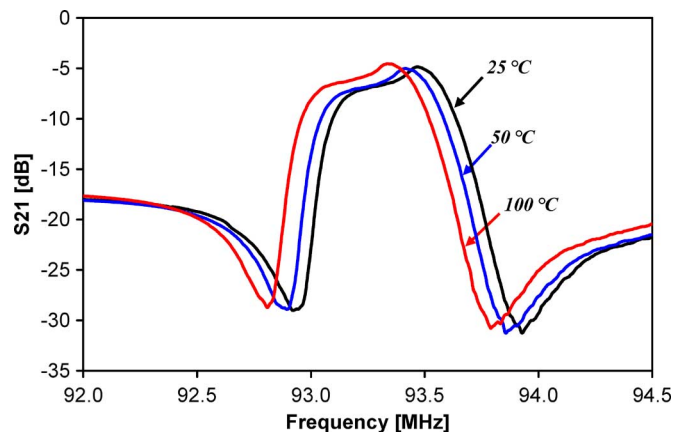

Fig. 16. Effect of temperature change (25–100 °C) on ladder filter composed of six rectangular plate resonators.

existing SAW and quartz crystal filters. Ongoing research is focusing on expanding the bandwidth of the filters, as well as introducing this technology into the GHz frequencies.

REFERENCES

[1] F. D. Bannon, J. R. Clark, and C.-C. Nguyen, "High-Q HF micro-electromechanical filters," *IEEE J. Solid-State Circuits*, vol. 35, pp. 512–526, 2000.
[2] W. Kun and C.-C. Nguyen, "High-order medium frequency microme-chanical electronic filters," *J. Microelectromech. Syst.*, vol. 8, pp. 534–556, 1999.
[3] W. Kun, F. D. Bannon, III, J. R. Clark, and C.-C. Nguyen, "Q-en-hancement of microelectromechanical filters via low-velocity spring coupling," in *Proc. Ultrason. Symp.* , 1997, vol. 1, pp. 323–327.
[4] S. A. Bhave, G. Di, R. Maboudian, and R. T. Howe, "Fully-differential poly-SiC Lame mode resonator and checkerboard filter," in *Proc. Int. Conf. Micro Electro Mech. Syst., (MEMS 2005)*, 2005, pp. 223–226.
[5] G. K. Ho, R. Abdolvand, and F. Ayazi, "Through-support-coupled mi-cromechanical filter array," in *Proc. Int. Conf. Micro Electro Mech. Syst., (MEMS 2004)*, 2004, pp. 769–772.
[6] S. Pourkamali, R. Abdolvand, G. K. Ho, and F. Ayazi, "Electrostati-cally coupled micromechanical beam filters," in *Proc. Int. Conf. Micro Electro Mech. Syst., MEMS 2004*, 2004, pp. 584–587.
[7] W. Ark-Chew and C.-C. Nguyen, "Micromechanical mixer-filters ("mixlers")," *J. Microelectromech. Syst.*, vol. 13, pp. 100–112, 2004.
[8] H. Chandrahalim, D. Weinstein, and S. A. Bhave, "Thickness shear mode vibrations in silicon bar resonators," in *Proc. Ultrason. Symp.*, 2005, pp. 898–901.
[9] S. A. Bhave and R. T. Howe, "Internal electrostatic transduction for bulk MEMS resonators," in *Proc. 2004 Solid State Sens., Actuator and Microsyst. Workshop*, 2004, pp. 59–60.
[10] ——, "Silicon nitride-on-silicon bar resonator using internal electro-static transduction," in *Proc. 13th Int. Conf. Solid-State Sens., Actua-tors and Microsyst. Transducers '05*, 2005, pp. 2139–2142.
[11] H. Chandrahalim, D. Weinstein, L. F. Cheow, and S. A. Bhave, "Channel-select micromechanical filters using high-K dielectrically transduced MEMS resonators," in *Proc. Int. Conf. Micro Electro Mech. Syst. (MEMS 2006)*, 2006, pp. 894–897.
[12] L. Yu-Wei, L. Sheng-Shian, X. Yuan, R. Zeying, and C. T. C. Nguyen, "Vibrating micromechanical resonators with solid dielectric capaci-tive transducer gaps," in *Proc. Freq. Control Symp. Expo.*, 2005, pp. 128–134.
[13] K. M. Lakin, J. Belsick, J. F. McDonald, and K. T. McCarron, "Im-proved bulk wave resonator coupling coefficient for wide bandwidth filters," in *Proc. Ultrason. Symp.* , 2001, vol. 1, pp. 827–831.
[14] R. Ruby, P. Bradley, D. Clark, D. Feld, T. Jamneala, and W. Kun, "Acoustic FBAR for filters, duplexers and front end modules," in *Proc. MTT-S Int. Microw. Symp. Dig.*, 2004, vol. 2, pp. 931–934.
[15] W. Kun, M. Frank, P. Bradley, R. Ruby, W. Mueller, A. Barfknecht, and M. Gat, "FBAR Rx filters for handset front-end modules with wafer-level packaging," in *Proc. Ultrason. Symp.*, 2003, vol. 1, pp. 162–165.
[16] K. Wang, W. Mueller, R. Ruby, M. Gat, P. Bradley, A. Barfknecht, F. Geefay, C. Han, G. Gan, A. Chien, and B. Ly, "High rejection Rx fil-ters for GSM handsets with wafer level packaging," in *Proc. Ultrason. Symp.*, 2002, vol. 1, pp. 925–929.

[17] P. Bradley, R. Ruby, J. D. Larson, III, Y. Oshmyansky, and D. Figueredo, "A film bulk acoustic resonator (FBAR) duplexer for USPCS handset applications," in *Proc. MTT-S Int. Microw. Symp. Dig.*, 2001, vol. 1, pp. 367–370.

[18] K. M. Lakin, "Bulk acoustic wave coupled resonator filters," in *Proc. Int. Freq. Control Symp. PDA Exhib.*, 2002, pp. 8–14.

[19] K. M. Lakin, J. R. Belsick, J. P. McDonald, K. T. McCarron, and C. W. Andrus, "Bulk acoustic wave resonators and filters for applications above 2 GHz," in *Proc. MTT-S Int. Microw. Symp. Dig.*, 2002, vol. 3, pp. 1487–1490.

[20] K. M. Lakin, "Coupled resonator filters," in *Proc. Ultrason. Symp.*, 2002, vol. 1, pp. 901–908.

[21] W. G. Cady, *Piezoelectricity; an Introduction to the Theory and Applications of Electromechanical Phenomena in Crystals*. New York: McGraw-Hill, 1946.

[22] R. A. Johnson, *Mechanical Filters in Electronics*. New York: Wiley, 1983.

[23] P. J. Stephanou, G. Piazza, C. D. White, M. B. J. Wijesundara, and A. P. Pisano, "Mechanically coupled contour mode piezoelectric aluminum nitride MEMS filters," in *Proc. Int. Conf. Micro Electro Mech. Syst., MEMS*, 2006, pp. 906–909.

[24] K. M. Lakin, G. R. Kline, and K. T. McCarron, "Thin film bulk acoustic wave filters for GPS," in *Proc. Ultrason. Symp.*, 1992, vol. 1, pp. 471–476.

[25] D. M. Pozar, *Microwave Engineering*, 3rd ed. New York: Wiley, 2005.

[26] A. I. Zverev, *Handbook of Filter Synthesis*. New York: Wiley, 1967.

[27] G. Piazza and A. P. Pisano, "Dry-released post-CMOS compatible contour-mode aluminum nitride micromechanical resonators for VHF applications," in *Proc. Solid-State Sensor, Actuator and Microsyst. Workshop*, Hilton Head, SC, 2004, pp. 37–40.

[28] H. Byeoungju, S. Insang, P. Yunkwon, K. Duckhwan, K. Woonbae, N. Kuangwoo, and P. J. Jungho, "Novel 1-chip FBAR filter for wireless handsets," in *Solid-State Sensors, Actuators and Microsyst., Transducers '05*, 2005, pp. 2069–2073.

[29] T. Ikeda, *Fundamentals of Piezoelectricity*. Oxford, U.K.: Oxford Univ. Press, 1990.

[30] W. Weaver, Jr., S. P. Timoshenko, and D. H. Young, *Vibration Problems in Engineering*. New York: Wiley, 1990.

[31] K. F. Graff, *Wave Motion in Elastic Solids*. New York: Dover, 1991.

[32] G. Ambati, J. F. W. Bell, and J. C. K. Sharp, "In-plane vibrations of annular rings," *J. Sound Vibrat.*, vol. 47, pp. 415–432, 1976.

[33] L. F. Mondolfo, *Metallography of Aluminum Alloys*. New York: Wiley, 1943.

[34] G. Piazza, "Piezoelectric aluminum nitride vibrating RF MEMS for radio front-end technology," Ph.D. dissertation, Univ. Calif., Berkeley, 2005.

Gianluca Piazza (S'00–M'06) received the Ph.D. degree from the University of California at Berkeley, in 2005.

He is an Assistant Professor with the Department of Electrical and Systems Engineering (ESE), University of Pennsylvania. His research interests focus on piezoelectric micro and nano systems (MEMS/NEMS) for RF wireless communications, bio/chemical detection, wireless sensor platforms, and medical ultrasounds. He also has general interest in the areas of micro/nano fabrication techniques and integration of micro/nano devices with state-of-the-art electronics. He developed a new class of AlN contour-mode vibrating microstructures for RF communications at the University of California, Berkeley. He has more than five years of experience working with piezoelectric materials, holds two patents in the field of micromechanical resonators and cofounded a start-up company (Harmonic Devices, Inc.) for the commercialization of piezoelectric resonators.

Philip J. Stephanou (M'05) received the B.S. and M.S. degrees from Rensselaer Polytechnic Institute, Troy, NY, in 2001 and 2002, respectively. His thesis investigated the performance of novel algorithms for computational multirigid-body dynamics.

He is pursuing the Ph.D. degree with the Mechanical Engineering Department, University of California at Berkeley, since 2002. His current research involves the analysis, design and fabrication of piezoelectric RF-MEMS resonators and filters for highly integrated communication systems. In spring 2005, he cofounded Harmonic Devices, Inc. (HDI), a fabless semiconductor startup committed to commercializing research breakthroughs in the area of RF-MEMS for the mobile handset market. He is currently the acting CTO of HDI.

Albert ("Al") P. Pisano received the B.S., M.S., and Ph.D. degrees from Columbia University, New York, NY, in mechanical engineering.

He currently serves as Professor and Chair of the Department of Mechanical Engineering, University of California at Berkeley (UCB). At UCB, he holds the FANUC Chair of Mechanical Systems in the Department of Mechanical Engineering, with a joint appointment to the Department of Electrical Engineering and Computer Science. He currently serves as a Director of the Berkeley Sensor and Actuator Center (BSAC). Prior to joining the faculty at UCB, he held research positions with Xerox Palo Alto Research Center, Singer Sewing Machines Corporate R&D Center, and General Motors Research Labs. From 1997 to 1999, he served as Program Manager for the MEMS program at the Defense Advanced Research Projects Agency (DARPA). His research interests and activities at UCB include MEMS for a wide variety of applications, including RF components, power generation, drug delivery, strain sensors, biosensors, and disk-drive actuators. He is the co-inventor listed on 20 patents in MEMS and has authored or coauthored more than 190 archival publications. He is a cofounder in start-up companies in the area of transdermal drug delivery, transvascular drug delivery, sensorized catheters, MEMS manufacturing equipment, and MEMS RF devices.

Dr. Pisano was elected to the National Academy of Engineering in 2001.